Protein-fluctuation-induced water-pore formation in ion channel voltage-sensor translocation across a lipid bilayer membrane

Suneth P. Rajapaksha, Nibedita Pal, Desheng Zheng, and H. Peter Lu

Protein Fluctuation Induced Water-Pore Formation in Ion Channel Voltage-Sensor Translocation across Lipid Bilayer Membrane

Suneth P. Rajapaksha, Nibedita Pal, Desheng Zheng, and H. Peter Lu*

Bowling Green State University, Department of Chemistry and Center for Photochemical Sciences, Bowling Green, OH 43402, USA

We have applied a combined fluorescence microscopy and single-ion channel electric current recording approach, correlating with molecular dynamics (MD) simulations, to study the mechanism of voltage-sensor domain translocation across a lipid bilayer. We use colicin Ia ion channel as a model system, and our experimental and simulation results show: (1) The open-close activity of an activated colicin Ia is not necessarily sensitive to the amplitude of the applied cross-membrane voltage when the cross-membrane voltage is around the resting potential of excitable membranes; and (2) there is a significant probability that the activation of colicin Ia occurs by forming a transient and fluctuating water-pore of ~15Å diameter in the lipid bilayer membrane. The location of the water-pore formation is non-random and highly specific, right at the insertion site of colicin Ia charged residues in the lipid bilayer membrane, and the formation is intrinsically associated with the polypeptide conformational fluctuations and solvation dynamics. Our results suggest a novel mechanistic pathway for voltage-sensitive ion channel activation, and specifically, for translocation of charged polypeptide chains across the lipid membrane under transmembrane electric field: the charged polypeptide domain facilitates the formation of hydrophilic water-pore in the membrane and diffuses through the hydrophilic pathway across the membrane; i.e., the charged polypeptide chain can cross a lipid membrane without entering into the hydrophobic core of the lipid membrane but entirely through aqueous and hydrophilic environment to achieve a cross-membrane translocation. This new mechanism sheds light on the intensive and fundamental debate on how a hydrophilic and charged peptide domain diffuses across the biologically-inaccessible high energy barrier of the hydrophobic core of a lipid bilayer: The peptide domain does not need to cross the hydrophobic core to move across a lipid bilayer.

1. INTRODUCTION

Ion channels are membrane proteins capable of regulating the ion flow across cell membranes. The channels are responsive to specific stimuli, for example, cross-membrane voltage change, ligand binding, local chemical composition change, mechanical stress, or light absorption [1-7]. Polypeptide domains with high charge densities, known as the voltage-sensitive peptides, are generally involved in voltage-gated ion channel activities. Typically, the conformational changes of a charged polypeptide domains under trans-

membrane voltage play critical roles in the voltage-gated ion channel open-close activations [8-10]. In recent years, it has been intensively debated on the mechanism and dynamics of moving a charged peptide chain across a lipid membrane. It has been estimated that the energy cost of pulling a charged peptide chain into the hydrophobic core of a lipid membrane is likely too high to occur under physiological conditions. For example, the free energy cost to insert an Arginine residue into the hydrophobic core of a lipid bilayer is estimated to be as high as 17 kcal/mole [11], and that for a voltage-sensor polypeptide domain can

be as high as 265 kcal/mol [12]. On the other hand, the experimentally measured energy barrier of inserting a voltage-sensor polypeptide is only ~2.5 kcal/mole [13]. The apparent discrepancy between the theoretical prediction and experimental finding compelled us to look for a deeper mechanistic understanding of the voltage sensor domain insertion and translocation across the lipid membrane. The fundamental question here is what is the dynamics and mechanism through which a charged peptide domain moves across the hydrophobic core of lipid membrane under a transmembrane electric field. Consequently, it can shed lights on some of the other fundamental questions like how to block a voltage-gated ion channel when they become permeable as a result of mutations [14].

In this paper we present a detailed study on colicin Ia channel unraveling a new mechanism of voltage-sensor domain diffusion through the hydrophobic core of a lipid bilayer. Although it is previously reported that the peptide translocation across the membrane can occur by forming a pore in the lipid membrane [14,15], there is a lack of comprehensive understanding about the mechanism involved in the process. Our results help to understand the mechanistic pathway of how a charged polypeptide chain can diffuse across the lipid membrane at low cost of activation barrier energy, much lower than the theoretically estimated energy of pulling a charged peptide into the hydrophobic core region of membrane. Intrinsically, peptide solvation dynamics plays a critical role in charged polypeptide chain translocation through the membrane as it is a well-established fact that the local solvation dynamics has a crucial role in maintaining protein's structure-function-dynamics relationship as well as conformational changes during folding and unfolding processes [16-18].

Here, we specifically study the voltage dependency of open-close activity of colicin Ia ion channel and translocation mechanism of the α-helices 2-5 of C-domain of colicin Ia across the membrane. We have developed and applied combined single ion channel electric current recording, fluorescence microscopic imaging, and molecular dynamics (MD) simulations study in this work. Colicin Ia is a monomeric-polypeptide with a single voltage sensor domain. Due to its simplicity, we chose colicin Ia ion channel as the

model system for our comprehensive study. Our experimental and computational results suggest that the conformational fluctuations of the colicin Ia under the transmembrane voltage can induce the formation of a hydrophilic water-pore across the membrane. The position of the water-pore is non-random but right at the insertion site of colicin Ia in the membrane, and the charged polypeptide domain moves across the membrane through the hydrophilic water-pore without entering the hydrophobic core region in process of the ion channel activation. Ultimately, our study provides a molecular-level answer to a critical question: what is the mechanism by which a large charged peptide domain translocates from external hydrophilic side of membrane through hydrophobic membrane core to the other hydrophilic side of the membrane? The answer of this question presumably has a significant implication in understanding the molecular mechanism of a range of voltage gated ion channel functions and dynamics [7,19-21].

Using colicin Ia in lipid membrane as the model system to study voltage sensor domain translocation

Colicin Ia, a water-soluble single subunit 69 kDa protein of 626 amino acids, is produced by *E. coli* bacteria [22-26] and only a single protein is needed to form an ion channel across a lipid bilayer membrane [27]. Colicin Ia has three main domains performing different functions (Fig. 1A): the T-domain, close to the N-terminal, translocates the protein across the outer cell membrane; the R-domain in the center binds to a receptor in the outer membrane; and the C-domain of ~175 amino acids forms a voltage gated ion channel in the inner membrane [6, 23-25,28]. These three domains are separated from each other by two long α-helices (Fig. 1A) [25]. The main function of the protein is carried out by the C-domain (blue in Fig. 1A) which forms the ion channel in the cell membrane [24,26,29,30]. The α-helices 8 and 9 in the C-domain mostly contain uncharged amino acids forming a hydrophobic hairpin (red in Fig. 1B) to embed in the hydrophobic core of the membrane thereby anchoring the C-domain [31,32], which is the initial step of the ion channel formation [33]. To form a functional ion channel under a transmembrane elec-

2
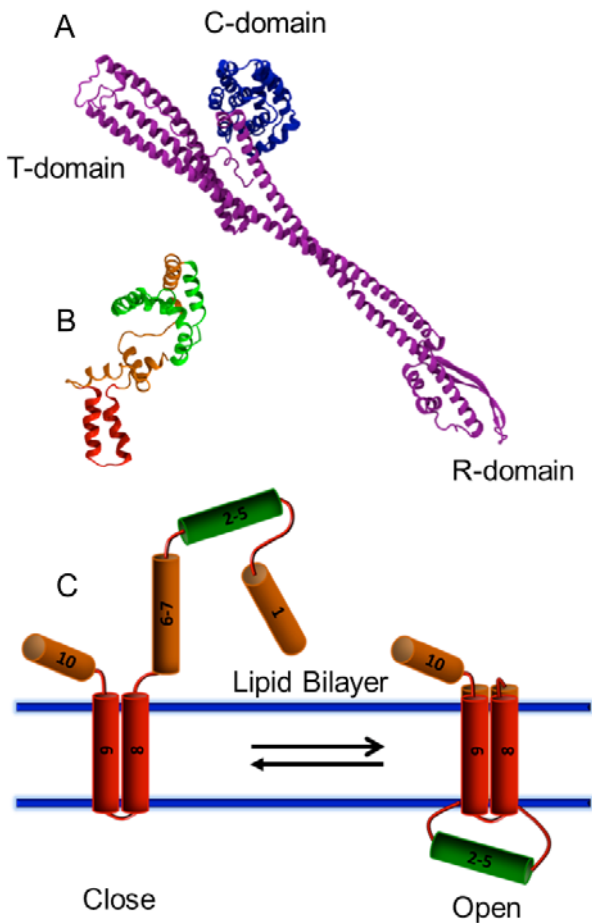
FIG. 1. (Color online) The structure of colicin Ia. (A) Colicin Ia protein. The channel forming C-domain is colored in blue and the rest of the protein is colored in purple. (B) The unwound C-domain of colicin Ia. Hydrophobic helices 8 and 9 are shown in red. The membrane crossing helices 2-5 are shown in green, and the other helices are shown in orange. The net charge of α-helices 2-5 is +7. (C) The open and close states of the ion channel, and the channel activation is related to the translocation of the α-helices 2-5 across the lipid bilayer, which leads the colicin Ia to form the ion channels under a transmembrane voltage.

tric voltage, the α-helices 2-5 (green in Fig. 1B) with a high density of the positively-charged amino acid moves across the cell membrane to bring the helix 1 and helices 6-7 into the membrane to join with the membrane-inserted helices 8 and 9 and form an active four-subunit ion channel (Fig. 1C) [6,33]. Although the translocation of helices 2-5 for the formation and activation of the ion channel is experimentally proved [6], the mechanism and dynamics of the translocation and channel's open-close activity are yet to be definitively characterized. Further exploration will ultimately lead us to a general understanding of the voltage sensitive ion channel activation and open-close activity [34,35].

2. MATERIALS AND METHODS

Materials

1,2-diphytanoyl-*sn*-glycero-3-phosphocholine (DPhPC) (Avanti Polar Lipids Inc. Alabama, USA) was used to prepare artificial lipid bilayers. KCl, NaOH, HCl, CaCl$_2$, *n*-Decane, HEPES (Aldrich) and Fluo 8H (AAT Bioquest) were used as received. The colicin Ia used in our experiments was purified, mutated, fluorescein-labeled and biotinylated by Prof. A. Finkelstein's group at the Albert Einstein College of Medicine, NY, and has only the C-domain (*the term "colicin Ia" in the materials and methods, and results and discussion sections refers to the C-domain of colicin Ia*). It has been reported earlier that the biotinylation of colicin Ia does not change its voltage gating characteristics [6], and it is most likely that the fluorescein labeling also does not change significantly the gating mechanism and dynamics of colicin Ia.

Single ion channel current recording

We prepared a horizontally suspended ~100 μm diameter DPhPC lipid bilayer to record single ion channel voltage-clamp current traces and correlated fluorescence imaging. A detail description of the bilayer preparation is published elsewhere [36]. Briefly, a horizontally suspended lipid bilayer was prepared at a ~100 μm diameter pinhole pathway by painting 10-20 mg/ml *n*-Decane solution of DPhPC in electrolyte solution of 1M KCl, 1mM EDTA, 5 mM CaCl$_2$, and 20 mM HEPES buffer of pH=8 [23]. After the insertion of colicin to the membrane, the single ion channel current was recorded with patch clamp amplifier (EPC7 *plus*, HEKA Electronik, Germany) filtered at 1 KHz. The data were recorded using LIH 1600 acquisition interface and PULSE V8.80 software (HEKA Electronik, Germany). Igor Pro (WaveMetrics, Inc.) and Matlab (MathWorks, Inc.) were used for the data analysis.

Single-Ion Channel Calcium flux fluorescence imaging

3

We used an established procedure to achieve the calcium flux fluorescence imaging by adding 0.1 M Ca^{2+} sensing dye [37] Fluo 8H to the *cis* side of the lipid bilayer, and adding 1M Ca^{2+} solution to the *trans* side of the lipid bilayer. The electrolyte used in this experiment does not contain any Ca^{2+}. The Fluo 8H dye molecules in the *cis* side emit fluorescence only after binding with Ca^{2+}. The lipid bilayer was illuminated with 488 nm laser beam (Argon ion laser, Melles Griot) in a wide-field epi-fluorecence imaging configuration [36-39]. The fluorescence signals were collected with an inverted microscope (Axiovert 200M, Zeiss) through a 60X water immersion objective (N.A. = 1.20). The collected photon signals from the sample was filtered with HQ505LP filter (Chroma Technology) and recorded with an EMCCD camera (Princeton Instrument, ProEM 512B).

Molecular Dynamics simulation

We used GROMACS v4.5.5 package (www.gromacs.org) to perform MD simulations with the extended united atom version of the GROMOS96 force field [40-44]. The membrane DPhPC bilayer model system and the modified parameters for lipids were used in our MD simulation [45-47]. Before inserting peptide, the only solvated DPhPC bilayer is simulated for 10ns in *NPT* (constant number of particles, pressure, and temperature) ensemble. The crystal structure of colicin Ia was downloaded from Protein Data Bank (PDB ID: 1CII) and edited to contain only the C-domain from 452 residue to 626 residue based on our examined molecules. Some of the single bonds in the loops of C-domain were rotated several degrees until we obtained a reasonable umbrella structure (Fig. 1B). After each rotation, the new structure was inspected to confirm that there were no conflicts between the coordination of the atoms. All energy minimization used less than 1000 steps of steepest decent method to remove any steric conflicts of the atoms. The helices 8-9 of the C-domain (red color segments in Fig. 1B) was embedded in the lipid bilayer by using the InflateGRO algorithm [48]. Then the system was solvated with 36,742 Simple Point Charge (SPC) waters and NaCl was added to the system at 0.1 M concentration [49]. Energy minimization was achieved by using less

than 1000 steps of steepest decent method to remove any steric conflicts of the atoms. After energy minimization, the system is slowly annealed in *NPT* ensemble over 500ps and then equilibrated for another 500ps in *NPT*. We used Nosé-Hoover thermostat at 323K for annealing, equilibration and rest of the simulation [50,51]. The MD simulation was performed at a constant temperature, constant pressure and constant number of molecules. The Parrinello-Rahman algorithm was used to couple the pressure at 1 bar throughout the simulation box [52,53] and the bonds were restrained using LINCS algorithm [54]. The long-range electrostatic interactions were calculated using the Particle Mesh Ewald (PME) method with a 1.2 nm cutoff for the real space calculations [55]. An electric field with appropriate strength correlating with the experimental condition was applied on the reverse z-direction. The integration time step was 2 fs, and the velocities and coordination of the each atom were saved in every 2 ps. The simulation was performed at Ohio Supercomputer Center, using 4 nodes with 10 processors per node. Molecular graphics were developed with Visual Molecular Dynamics (VMD) [56].

Combined fluorescence imaging, single channel electric recording and MD simulation approach

Combined single ion channel electric current recording and fluorescence microscopic imaging are capable of characterizing the mechanism and dynamics of ion permeable pore formation, cellular response, ion channel functions and related conformational changes [37,39,57-60]. Furthermore, MD simulations play a complimentary role in achieving a molecular-level analysis of ion channel formation and activity dynamics [61-67]. In recent years, theoretical calculation and MD simulation have been extensively applied to study biological membrane, membrane associated protein dynamics and biomolecular recognition [48,68-72]. For example, the MD simulation studies of the insertion of α-helices into the membrane and stability of α-helices in the membrane have been reported [73-76]. Although these studies have provided insightful information about the specific or generalized ion channels, the details of colicin Ia have not been studied with MD

4

simulations largely due to the lack of experimental structural and dynamic information of the ion channel's membrane-bound states [77]. Nevertheless, in this work, we compared simulation results to the experimental findings to develop a molecular level picture of peptide translocation across lipid membrane while forming an active ion channel.

3. RESULTS AND DISCUSSION

Understanding the ion channel open-close activity dynamics and mechanism: Activated ion channel open-close state dynamics is primarily driven by stochastic thermal fluctuations of the ion channel's peptide conformations in the membrane

We recorded the single ion channel current and conductance fluctuations of colicin Ia channel gating at three different transmembrane voltages; 50 mV, 70 mV and 100 mV (Fig. 2: A1, A2 and A3, respectively). The single ion channel conductance trajectories clearly show the ion channel close state at the lower level and open state at the higher level. The ion channel open and close states are identified by using a threshold value based on the lowest populated conductance in the conductance distribution. A state with conductance value higher than the threshold is considered to be the open state, and a state with conductance value lower than the threshold is considered to be the close state.

We have analyzed the ion channel open-close activity dynamics by calculating autocorrelation function from the recorded single ion channel conductance time trajectories [37,38].
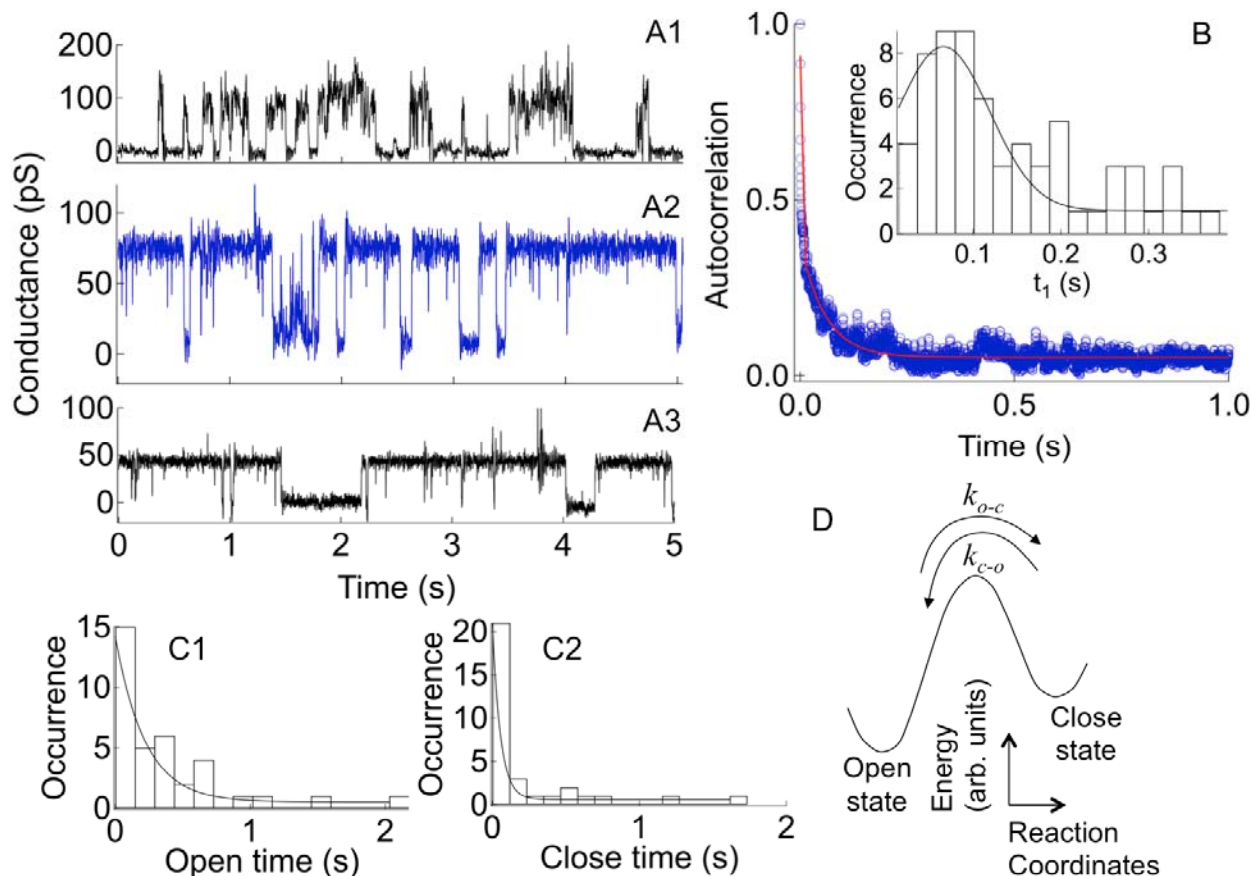
FIG. 2. (Color online) The single ion channel conductance trajectories and analysis. (A) The 5s long conductance trajectories at: (A1) 50mV (A2) 70mV (A3) 100mV and (B) The autocorrelation function analysis of the conductance trajectory under 70 mV transmembrane voltage. The bi-exponential decay fitting is shown in red. The faster time component of the decay is 0.093s. (*Inset*) The distribution of the faster time component (t_1) of the autocorrelation function decay fitting is based on 59 trajectories recorded at 70mV. The mean of the Gaussian fitting is 0.066±0.018s. (C1) The distribution of the channel open times with mean at 0.23±0.05s at 70mV. (C2) The distribution of the channel close times with mean at 0.043±0.005s of a 20s long conductance trajectory at 70mV. (D) The potential energy surface diagram of the colicin Ia ion channel. k_{o-c} is the transition rate of open to close and k_{c-o} is the transition rate of close to open.

$$C_{auto}(t) = \langle \Delta A(0) \Delta A(t) \rangle \big/ \langle \Delta A(0)^2 \rangle = \langle (A(0) - \langle A \rangle)(A(t) - \langle A \rangle) \rangle \big/ \langle (A(0) - \langle A \rangle)^2 \rangle$$

where $A(t)$ is the signal variables, the conductance, measured from a single ion channel. $<A>$ is the mean conductance of the fluctuation trajectory. Fig. 2B, 2C1 and 2C2 show the autocorrelation analysis of the conductance trajectories recorded at 70mV. The recorded continuous conductance trajectories are divided into 5s segments (Fig. 2A), and the autocorrelation function of each trajectory is calculated and the decay time is analyzed (Fig. 2B). The autocorrelations of the conductance follow bi-exponential decay dynamics essentially due to complex interaction of the ion channel helices with themselves and surrounding local environment that ultimately produce slower and faster time components. The temporal distribution of the slower time component is considerably broad, from milliseconds to seconds, possibly involving some stochastic dynamics of the protein. Furthermore, the narrow faster time distribution gives the mean ($\tau_{o \leftrightarrow c}$) at 0.066±0.018 s (Fig. 2B *inset*). $\tau_{o \leftrightarrow c}$ is the total time needed for a single event of channel's open-close transition. Inverse of $<\tau_{o \leftrightarrow c}>$ is the rate for open-close transition ($K_{o \leftrightarrow c}$) and equal to the sum of the channel's open to close rate ($k_{o-c}=1/\tau_o$) and close to open rate ($k_{c-o}=1/\tau_c$) [78].

$$K_{o \leftrightarrow c} = k_{o-c} + k_{c-o} \qquad (1)$$

The dwell times of the channel in the open state (τ_o) and the close state (τ_c) are calculated by using 20s long conductance trajectories. Using the threshold as we have discussed above, we are able to read out the dwell times of the open and close states from each single ion channel conductance trajectory. Fig. 2C1 and 2C2 show the distribution of the read-out open dwell times and close dwell times, respectively, and the distribution shows typical Poisson temporal distribution feature of exponential decays. We separately calculated the average open dwell time ($<\tau_o>$) and average close dwell time ($<\tau_c>$) and further calculated the ratio of $<\tau_o>/<\tau_c>$. The inverses of these dwell times are the average rate of open to close transition ($1/ <\tau_o>=<k_{o-c}>$) and average rate of close to open transition ($1/ <\tau_c>=<k_{c-o}>$) (Fig. 2D) [79]. We have $<k_{o-c}>/<k_{c-o}>$ ratio to be 0.194. Since the total rate ($1/<\tau_{o \leftrightarrow c}>=K_{o \leftrightarrow c}$) is 15.2 s^{-1},

we calculate the k_{o-c} and k_{c-o} to be 2.47 s^{-1} and 12.7 s^{-1}, respectively. The same calculation procedure is followed for the conductance trajectories recorded at 50 mV and 100 mV transmembrane voltages. At 50 mV, k_{o-c} and k_{c-o} are 3.17 s^{-1} and 9.66 s^{-1}, respectively, and at 100 mV, k_{o-c} is 2.14 s^{-1} and k_{c-o} is 7.83 s^{-1} (see Ref. [80]).

We observed that the transmembrane voltage is a basic requirement for the starting of the channel open-close activity. Our results show that the most active ion channel is formed with +70 mV electric field, which is near the resting potential of typical excitable cell membranes. In the presence of external voltage across the membrane, the helices 2-5 in the *cis* side of the bilayer can drift through the lipid membrane, allowing the protein to form an activated ion channel. However, after the ion channel is formed and activated, the open-close activity is likely to have less dependency on the applied electric field. The rate from open to close is slightly decreasing with increasing the voltage while the rate of close to open maximizes at +70 mV transmembrane voltage. We attribute that at +70 mV, the resting potential of the excitable membranes, the force applied on the helices 2-5 segment is the optimal force to keep the voltage sensitive segment of the protein at the position in *trans* side of the membrane to form the activated ion channel. Lower or higher than +70 mV voltage does not necessarily provide the range of external force needed for helices 2-5 to undergo conformational change in order to form an effective ion channel. The rates of open to close and close to open processes are approximately in the same range, implying the protein's less dependency on the applied transmembrane voltage for its open-close activity. We suggest that, after the channel is formed in membrane, the ion channel open-close activity is essentially driven by thermally-driven conformational fluctuations of the ion channel and its local membrane environment. As suggested by the literature [81-84], the protein conformational changes or protein folding such as open-close transition of the ion channels can be a non-Arrhenius process which has a considerably lower activation barrier energy, 2.8-3.1 kcal/mole, than the 13.4-16.0 kcal/mole calculated by using the Arrhenius relationship at the same ambient temperature, assuming the pre-exponential factor to be 10^{11} to 10^{13} s^{-1}, respectively [81-84]. How-

ever, the exact quantitative correlation between thermally driven conformational fluctuations and the electric current on-off changes demands further structural studies, which is beyond the scope of this work. After the formation of the ion channel, the existing transmembrane voltage mostly serves as a biased field to keep helices 2-5 in the *trans* side, rather than driving the channel open-close conformational motions. The only voltage-dependent processes in the colicin Ia ion channel formation involves the translocation of the α-helices 2-5 across the membrane, bringing the α-helices 1, 6-7 into the membrane to join with helices 8 and 9 to form the channel configuration, and keeping the translocated helices 2-5 in the *trans* side of the membrane.

Identifying ion channel activation dynamics and mechanism: revealing a new pathway of voltage sensor domain peptide translocation across a lipid bilayer membrane

Based on our experimental results and above discussion, we attribute that the translocation of helices across the membrane happens only at the activation on-set time in a single channel open-close time trajectory. Nevertheless, the question still remains: how does a large and charged polypeptide domain move across the lipid bilayer from one hydrophilic side through a hydrophobic inner layer to the other hydrophilic side of the membrane to form an activated colicin Ia channel? The answer to this question may provide a new understanding of the molecular mechanism of voltage gated ion channel functions and dynamics [7,19-21].

The recorded conductance trajectories of single colicin Ia channel (Fig. 3A) clearly show the channel close state at a lower conductance level and the channel open state at a higher conductance level in the presence of transmembrane electric field. The average conductance of the single channel is 70±1.9 pS (Fig. 3B), consistent with the reported conductance of a typical single colicin Ia ion channel [24].

It is intriguing that colicin Ia ion channel open-close activity starts with a transient high conductance signal (THC) (Fig. 3A). The occurrence of the THC state is temporally non-random and highly correlated with the onset of the channel open-close activity, i.e., the channel activation onset events. We have observed the probability of THC state occurrence is about 40±10% amongst our recorded single ion channel conductance trajectories when individual active colicin ion channels are formed, i.e., there is a strong temporal correlation between the THC state appearance events and the onset of the single ion channel open-close activities. The THC state appears likely to be a precursor event associated with the colicin channel activation. In our experiments, the conductance trajectories of the colicin Ia are recorded under a constant voltage without amplitude and polarity changes, i.e., the transmembrane voltage is applied long before the appearance of THC state. Therefore, the transient THC signal cannot be resulted from polarization and depolarization or charging and discharging of the lipid bilayer, namely, the typical Faraday charging effect. Furthermore, our data also show that the dynamics of the THC state appearance typically involves multiple steps and significant fluctuations (Fig. 3C). Presumably, the channel open-close activity starts with the formation of the ion channel, and the channel formation is related with the translocation of the α-helices 2-5 across the lipid bilayer under the transmembrane voltage of +70 mV (Fig. 1C) [6,23]. We attribute that the origin of the transient THC state is the formation of a larger water-pore through which the helices 2-5 diffuses across the membrane to form a colicin Ia ion channel in the lipid bilayer.

The mean of the conductance distribution of the THC states is 310±13 pS (Fig. 3B & 3D). Assuming the conductivity (σ) and the thickness of the lipid bilayer membrane (l) are constants for a given system during the time of the measurements, the conductance (G) depends only on the size (cross section area, A) of the pore pathway, as $G = \sigma A / l$. Therefore, we estimate the average cross sectional area of the THC pore pathway is about 4.5 times larger than the cross sectional area of a regular open colicin channel. According to the previously reported channel structure, the channel is hourglass-shaped, with a ~18 Å diameter entrance in *cis* side, a ~10 Å diameter entrance in *trans* side and a ~7 Å diameter narrowing between the entrances [85]. Considering the ~7 Å limiting diameter of the channel, the average cross sectional area of the THC pore is calculated to be 170.5 Å^2 [6], and the diameter is ~15

7
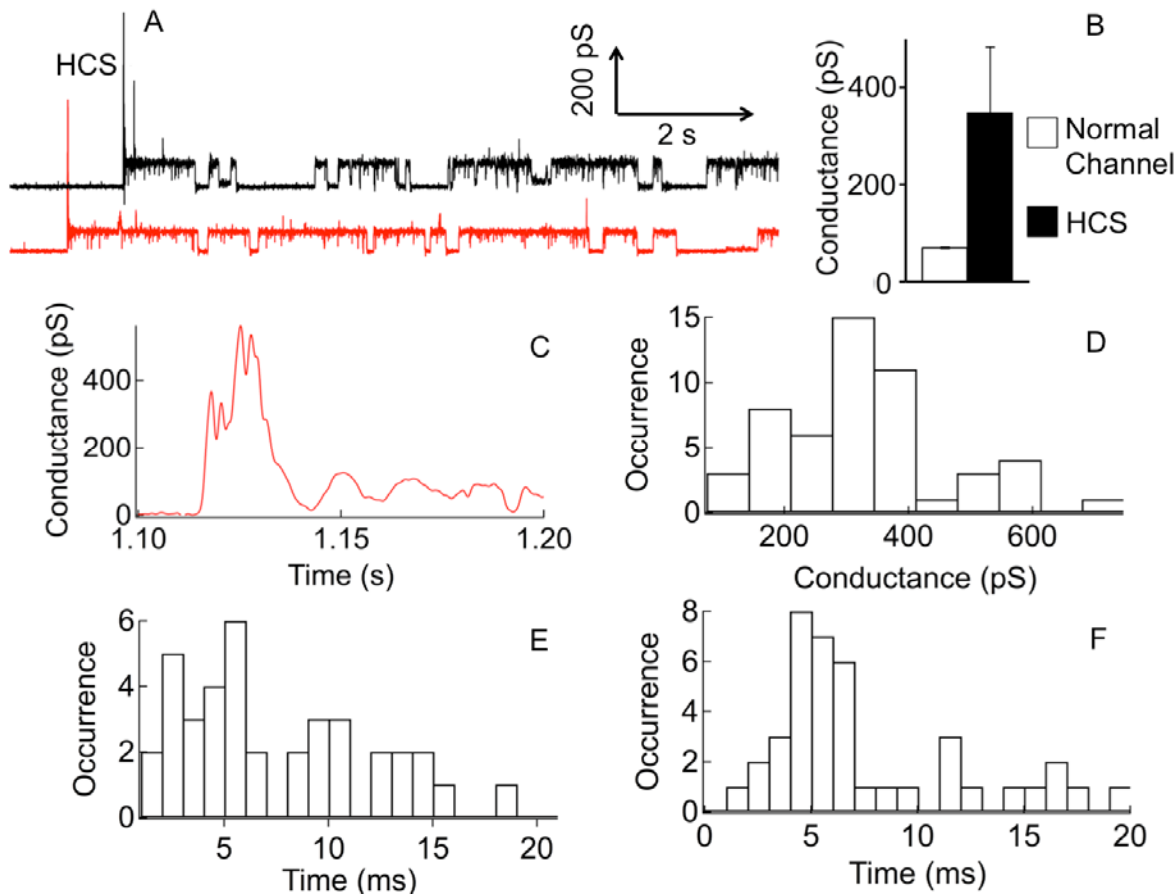
FIG. 3. (Color online) High conductance trajectory analysis. (A) Conductance trajectories of single channels. Both *black* and *red* trajectories were recorded under a constant +70 mV transmembrane voltage. The normal ion channel conductance is reached after the appearance of a transient high conductance (THC) state. (B) The average conductances of the normal channel and THC state. *White* is the average conductance of the normal ion channel, 70±1.9 pS (based on 12 trajectories). *Black* is the average conductance of the THC state, 348±135 pS (based on 52 THC states). (C) The zoom-in view of the THC state of the *red* trajectory in A. It is apparent here that the THC state does not appear as a single spike. (D) The conductance distribution of the THC states. The mean conductance of the THC states is 310 pS from the distribution calculated from 52 trajectories. (E) The distribution of the open times of the THC state. The mean open time is 3.48 ms from the distribution calculated from 41 trajectories. (F) The distribution of the close times of the THC states. The mean close time is 4.47 ms from the distribution calculated from 52 trajectories. Therefore the average time of the THC state appearance in the membrane is 7.95 ms.

Å. Based on the data of a large number of recorded single ion channel activation events and single ion channel electric recording trajectories, we have also calculated the distributions of open time and close time of transient THC state (Fig. 3E and 3F), and the average lifetime of the observed THC states is found to be 8.0 ±0.1ms.

Correlated single channel fluorescence microscopic imaging and single channel electric recording to identify the hydrophilic water-pore pathway associated with the channel activation

To further identify that the THC state is due to the formation of a water-pore pathway in the membrane correlated with the ion channel activation, we have conducted a control experiment using Ca^{2+} flux imaging correlated with single ion channel current recordings [86]. Fig. 4A1-4A5 show the consecutive five imaging frames of optical measurement, each with 3 ms exposure time, recorded during an ion channel activation event. A relatively brighter spot in the fluorescence imaging, indicating a high Ca^{2+} current and accumulation at the spot, appears (Fig. 4B) in correlation with the THC state appearance (Fig. 4C). It is apparent that the electric conductance

8
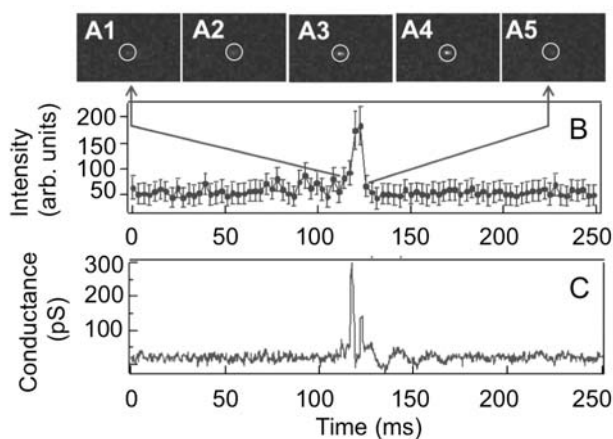
FIG. 4. Correlated fluorescence imaging and single ion channel current recording studies of the formation of the THC. (A) Consecutive five frames of Ca^{2+} imaging where the opening of the lipid bilayer is observed correlated with ionic current measurement. The white circle shows the position of the brighter spot. The images were collected with 3 ms exposure time in a 100×33 binned pixels area where each pixel in the image represents 2×4 pixels, and the binning of the pixels was done to keep the readout time less than exposure time. (B) Correlated fluorescence intensity trajectory recorded by the fluorescence imaging. Error bar shows the standard deviation. (C) Correlated ion channel conductance trajectory recorded by ion channel voltage clamping recording. The trajectory only shows the THC state but without significant on-off electric activity follows, which benefit a clear optical imaging of low fluorescence background.

increases as the brighter imaging spot appears in the correlated recording, and the electric conductance drops back to the background level and the brighter spot disappears at the same time, showing a strong temporal correlation between the fluorescence imaging and electric conductance trajectories. The correlation between the increased fluorescence intensity and electric conductance suggests that the water-pore pathway formation in the lipid bilayer is the origin of the THC state appearance leading to the activation of colicin Ia channel and following open-close activities. Furthermore, the images in Fig. 4A2-4A4 cannot be due to a random leak of Ca^{2+} through the membrane or an already activated ion channel, because there is no observable imaging signal intensity above the background in Fig. 4A1 and 4A5 before and after the THC state occurrence event recorded simultaneously by single-ion channel electric conductance detection (Fig. 4).

MD simulation analysis of voltage sensor domain of ion channel protein translocation across the lipid bilayer membrane

To obtain a further molecular-level understanding of the charged peptide domain translocation across a lipid bilayer through a possible water-pore associated with the THC state occurrence, we have conducted MD simulations with C-domain of colicin Ia under a transmembrane electric field. In recent years, MD simulations have emerged as a powerful approach to compliment the experimental findings by providing detailed insight about translocation of bio- and inorganic molecules through lipid membranes [87-89]. We note that the aim of our MD simulation is to have a conceptual and qualitative understanding of the charged peptide diffusion across a lipid bilayer under a transmembrane voltage rather than exactly simulating the experimental results of colicin conformational dynamics in the ms-to-min time scale.

The umbrella conformation of the C-domain (Figure 1B) is used as the starting configuration of colicin Ia due to its reported lowest free energy amongst all the accessible conformations [77]. The DPhPC lipid bilayer model is constructed and simulated as discussed above. The MD simulation started with a 0.07 V/nm transmembrane electric field and is increased to 0.15 V/nm at 23 ns and maintained at that value throughout the rest of the simulation.

The simulation has evidenced that the translocation of the charged peptide domain across the hydrophobic lipid membrane is associated with a water-pore formation right at the peptide insertion site and across the lipid bilayer. Initially the water molecules penetrate stochastically the core of the hydrophobic bilayer to form a wire-like path (Fig. 5A1 and 5A2). As time passes the wire-like structure grows in size and expands to form a water filled hydrophilic pore (Fig. 5A3) that provides a polar pathway for charged residues to translocate across the lipid membrane. We emphasize that the location of the water-pore formation is not random, but rather highly correlated to the site of the charged peptide residues in the membrane. We have run adequate number of trajectories, and we have also run a number of trajectories by using different lipid bilayer, such as DPPC (1,2-dipalmitoyl-*sn*-

glycero-3-phosphocholine) lipid bilayer (data not shown). In all the simulated trajectories, we observed that the water-pore is formed right under the peptide domains containing charged amino acids. In all cases the water-wires appear from both side of the lipid bilayer and they extend to join to form the water-pore (Fig. 5). Several earlier studies reported that transmembrane segments containing charged residues, e.g., Arginine or Aspartic acid, induce deformation in the membrane either by dragging water molecules along with them or by snorkeling, thereby allowing water molecules to penetrate bilayer [90-94]. The presence of extra protein content inside bilayer further facilitates charged residues in retaining its hydration layer [91]. Likewise, in our system, the fluctuation of helical hairpin segment (helices 8 and 9) inside the lipid bilayer likely induce some local deformation in the opposite side lipid leaflet through which interfacial waters seep deeper in the interfacial region while still maintaining the structural integrity of the lipid bilayer. This deformation is further enhanced as charged voltage sensor domain drags more water molecules with it in retaining its energetically accessible hydration. At the later stage, lipid head groups reorient themselves sparsely to margin the water-pore thus stabilizing the water-pore [80].

The characteristics of lipid bilayer, i.e., the thickness and the density of lipid appear to be highly correlated with the water-pore formation. We have calculated the thickness of the lipid bilayer during the formation of the water-pore pathway across the membrane using GridMAT-MD [95] and results are shown in Fig. 6A. The thinning of the lipid bilayer near charged peptide residues is first observed after 58 ns, which continues throughout the rest of the simulation as the water-pore increases in size (Fig. 6A). Furthermore, the density of DPhPC molecules and water molecules in the membrane normal direction also show significant variations during the water-pore pathway formation (Fig. 6B1 and 6B2). Before the water wire appears, no water molecule is present in the hydrophobic core region between the two DPhPC leaflets. When the water wire occurs, the density of water molecules dramatically increases with time. This corresponds to the formation of the water filled pore pathway. The density of DPhPC shows the inverse behavior compared to the water molecule density (Fig. 6B2). We note that as the local region becomes
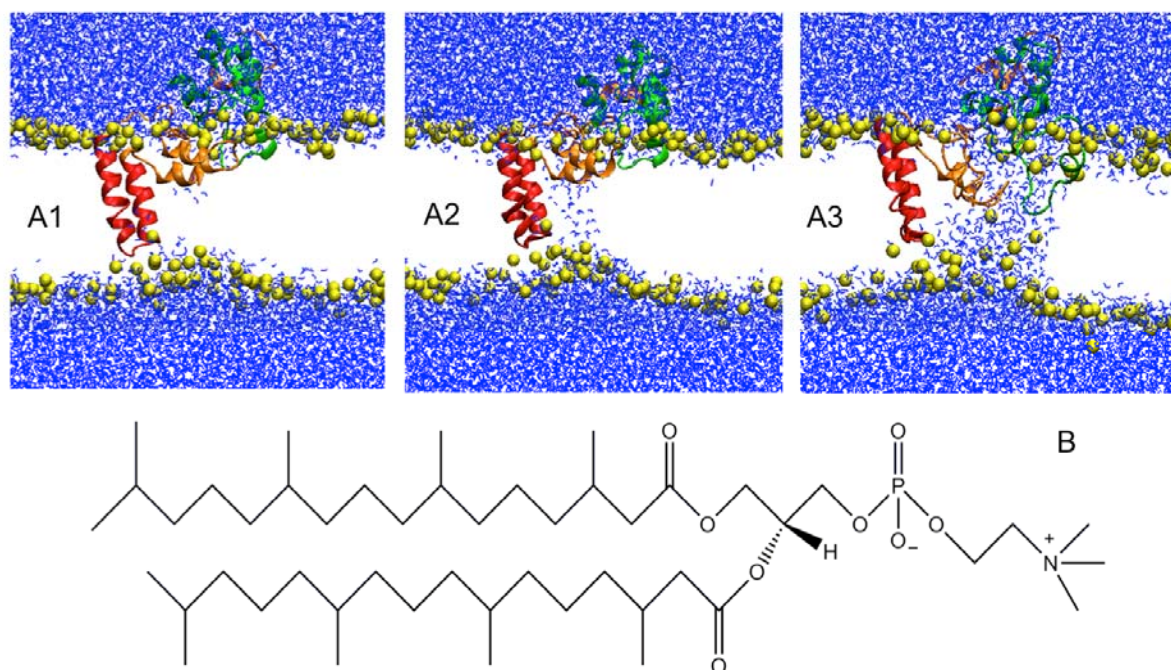
FIG. 5. (Color online) MD simulation snap shots of colicin Ia in the 1,2-diphytanoyl-*sn*-glycero-3-phosphocholine (DPhPC) lipid bilayer under transmembrane electric field. (A) Formation of the water filled pore pathway by C-domain driven under electric field. Here we use only the phosphorus atom (yellow) to represent the lipid molecules. (A1) The deformation of the lipid bilayer starts under the charged peptide domains and water molecules from both side of the bilayer start entering into the lipid bilayer (58 ns). (A2) The appearance of the water-wire across the DPhPC bilayer (63 ns). (A3) The formation of a larger water-pore pathway across the lipid bilayer (76 ns). (B) Chemical structure of DPhPC molecule.

thinner to form the water-pore pathway, the other area around of the water-pore pathway region shows an increasing or unchanged thickness of the DPhPC membrane as what the green curve shows in Fig. 6B2. The thickness changes are consistent with the increasing entropies of water and the DPhPC molecules [96]. We stress here that our MD simulation finding only qualitatively supports our experimental findings. To make a quantitative or semi-quantitative correspondence with the experimental results, we need long simulation run to calculate pore formation dynamics and structural calculation, which is technically beyond the scope of this work.

To rule out electroporation, i.e., the possibility of water-pore pathway formation in a lipid bilayer by an external electric field alone [97,98], we have used significantly lower electric fields for our simulation than that of previously reported minimum strength required for electroporation [99-102], and the water-pore pathway is not formed at a random location but rather a highly specific location right under the charged residues of the colicin Ia (Fig. 5 and 6). To check

further, we ran MD simulation on bare DPhPC bilayer with 0.15 V/nm electric field. We did not notice any signature of water-pore formation even after 125 ns [80]. The phenomenon of electroporation at such low electric field may take hundreds of ns to initiate. As we see water-pore formation to start ~50 ns with such low electric field in our system, we can certainly rule out the possibility of electroporation when colicin is inserted in lipid bilayer. In a separate MD run, we switched off the electric field after a sufficiently large water-pore is formed (78 ns here) to observe whether it leads to membrane reconstruction. We did not run long enough simulation to observe the complete membrane resealing; however, we did observe the decrease in water-pore size [80]. It is to be noted that the membrane reconstruction process in our present system may take much longer time compared to previous reports [103] as the water-pore gets stabilized due the interaction of counter ions with the lipid head group. Additionally, we also checked whether peptide-membrane interaction in the absence of any transmambrane electric field could initiate
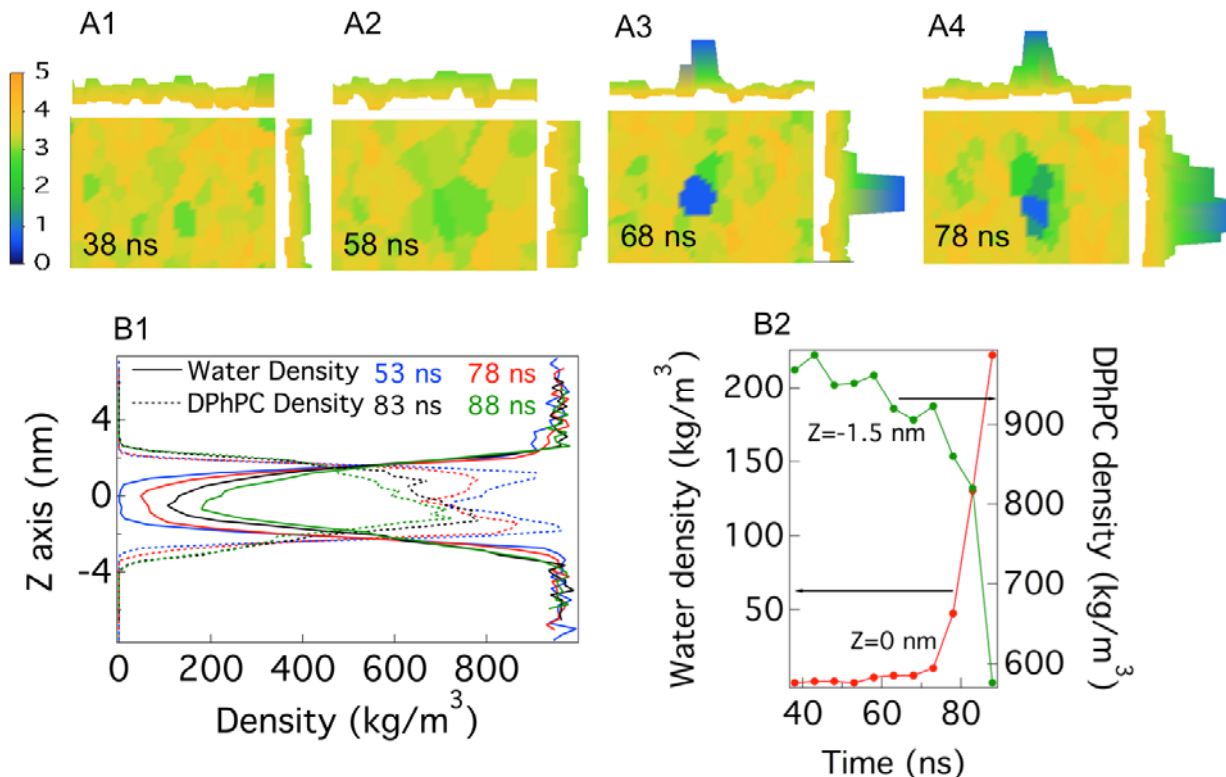
FIG 6. (Color online) MD simulation of colicin Ia in the DPhPC lipid bilayer under transmambrane electric field. (A) The thickness variation of the lipid bilayer (in nm) with time during water-pore formation. (B1) Density of the water molecules and DPhPC molecules in slabs along Z-axis of the simulation box (membrane normal direction). (B2) Density variation of water molecule of specific slab with center located at Z= 0 nm and density variation of DPhPC molecules of specific slab located at Z=-1.5 nm.

the water-pore formation. For that purpose, we ran MD simulation without any transmembrane electric field while C domain of colicin Ia is inserted in the lipid membrane. Even after 80 ns of MD run, we did not see any signature of water-wire or water-pore formation [80]. Although cationic peptides are found to be responsible for membrane disruption by interacting specifically with negatively changed lipid membrane at moderate to high protein to lipid molar ratio [104], in our system, the zwitterionic nature of DPhPC bilayer with very low protein to lipid molar ratio could be the reason for no initiation of water-pore formation without transmembrane electric field. Therefore, based on all of the control experimental and computational results, we attribute the formation of the water-pore to be uniquely induced by the polypeptide, especially the charged voltage-sensor residues of colicin Ia under the transmembrane electric field.

In our experimental measurements discussed above, it takes hundreds of milliseconds to minutes for the formation of the water filled pathway before the colicin polypeptide voltage-sensor segment diffuses across the lipid membrane. However, in our MD simulation the applied electric field is 3.5 to 7.5 times higher than the previous reports [97,98]. The reason behind is to initiate the water-pore formation in a shorter time scale while still showing the essentially same characteristics. It is expected that the water-pore formation in lower electric field would be much slower in our MD simulation but would still occur. Nevertheless, the essential physical nature of the water-pore pathway formation induced by the voltage-sensor domain of the colicin Ia is characterized in our MD simulation, suggesting that the charged residue regions of colicin Ia promotes the deformation of the lipid bilayer thereby acting as a precursor for the water filled hydrophilic pathway formation. Highly specific and non-random location of the water-pore right under the voltage sensor peptide domain further corroborates this finding.

Overall, our MD simulation serves as a qualitative or semi-quantitative control on the interpretation of our experimental results, which suggests that (1) there are early events that lead to a propensity of water-pore formation; (2) the water-pore formation is completely non-randomly but right at the site in the lipid membrane where the charged peptide domain resides; and (3) the charged peptide domain diffuses across the membrane through the hydrophilic water-pore. Our MD simulation in particular or a typical MD simulation may not be able to observe a stable water-pore at its equilibrium state, as it is most likely that the charged peptide diffuses across a transient water pore is a highly dynamic process in nature. We note that we have run MD simulation with the same starting structure of colicin Ia inserted in DPhPC bilayer but without an applied transmembrane electric field. We did not observe any signature of water-pore
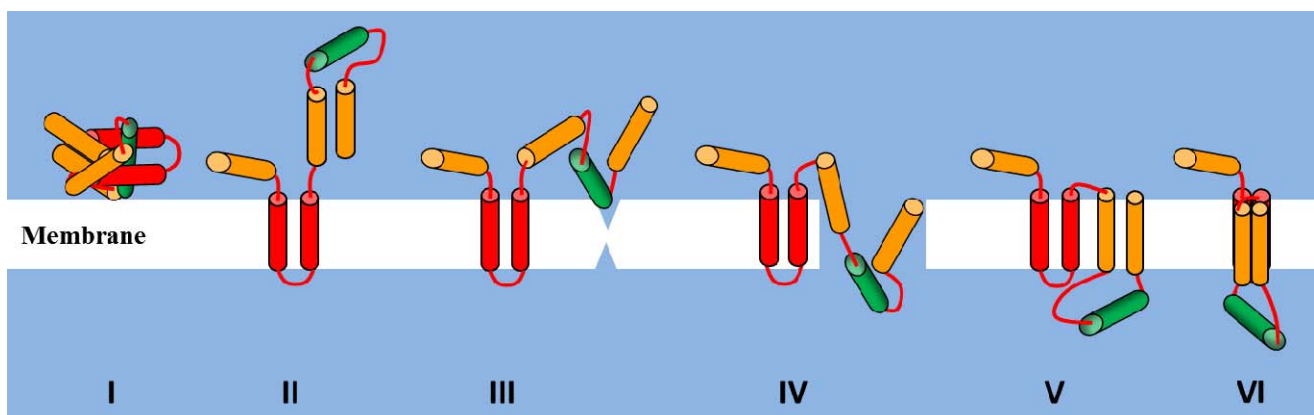
FIG. 7. (Color online) The model for the diffusional translocation of the α-helices 2-5 (green) across the hydrophobic lipid bilayer (Color scheme as Fig. 1C). **(I)** Adsorption of the colicin Ia onto the lipid bilayer. **(II)** The umbrella structure of colicin Ia. Hydrophobic (red) segment has inserted into the lipid bilayer. **(III)** Formation of water wire inside the lipid bilayer. **(IV)** Formation of a large hydrophilic water-pore pathway and translocation of the helices 2-5 of the colicin Ia across the lipid bilayer. **(V)** After translocation, the water-pore disappears due to a spontaneous membrane self-repair, and the helices 1, 6-7, 8 and 9 are positioned inside the lipid bilayer. **(VI)** The formation and activation of the normal ion channel.

formation even after 80 ns whereas water-wire starts forming under the applied transmembrane field at ~50 ns. To make a quantitative or semi-quantitative correspondence with the experimental results, namely, equilibrium open-close dynamics, there is a need for much longer simulation run, which is beyond the scope of this work.

New model of voltage sensor domain transmembrane motions

The model for the formation of the colicin Ia channel in a lipid bilayer was first proposed by Kienker *et al.* [33], describing (1) adsorption of the C-domain to the membrane; (2) orientation of the α-helices 8-9 and their insertion into the membrane; (3) formation of the ion channel through the charged voltage-sensor helices 2-5 translocation across the membrane driven under a transmembrane voltage. However, thus far, neither this model nor any other reported works have identified or described the specific mechanism and dynamics of the channel open-close conformational motions and helices 2-5 translocation across the membrane. According to the conventional mechanism, channel open and close events are mostly regulated by transmembrane voltage. Also, the charged polypeptide domain presumably involves solvation and desolvation as it moves from one hydrophilic side to another hydrophilic side crossing the hydrophobic core of the membrane. However, the question remains how a charged polypeptide can cross the energy barrier to move inside the hydrophobic core of the membrane. Because, it is well known that there is not enough energy is available for such desolvation and interaction between the hydrophilic and charged polypeptide domain with the hydrophobic core of the lipid tiles in the membrane, even under the drive of the transmembrane voltage. Based on our experimental and MD simulation results, we are now able to provide a new insight about the colicin Ia channel open-close events and water filled pore formation pathway for identifying how the charged domain of colicin Ia (helices 2-5) diffuses crossing the hydrophobic core of the lipid bilayer to form the four subunit ion channel. We propose a modified model for translocation of the colicin Ia α-helices 2-5 across the membrane (Fig. 7): (1) After being introduced to *cis* solution, the colicin Ia diffuses randomly before it comes onto and gets adsorbed on the lipid bilayer (Fig. 7I); (2) Then the hydrophobic hairpin inserts into the lipid bilayer, generating the umbrella structure (Fig. 7II); (3) Driven by the external transmembrane electric field, charged residues of colicin Ia induce a deformation in the lipid bilayer, directing the water to form conical intrusions into the lipid bilayer, starting as a water wire across the membrane (Fig. 7III); (4) The water intrusions, along with the solvation layer of the charged polypeptide segment, form a larger hydrophilic pore that provides a polar and aqueous pathway for the charged residues of colicin Ia to diffuse across the hydrophobic lipid bilayer under the driving force of the 70 mV transmembrane voltage (Fig. 7IV); (5) In the following step of the ion channel activation, the pore pathway closes while having four helices in the lipid bilayer and the α-helices 2-5 in the *trans* side of the lipid bilayer (Fig. 7V); (6) In the final step, the four helices form the channel of colicin Ia (Fig. 7VI), which produces open and close states mostly due to the ion channel's conformational fluctuations driven by local thermal fluctuations. Nevertheless, the core element of the energetics and dynamics of the ion channel activation is the solvation of colicin polypeptide domain by hydrophilic water and hydrophobic lipid molecules under an external transmembrane voltage [99-102]. Overall, according to our new mechanism, the charged polypeptide domain actually does not involve a significant solvation-desolvation dynamics but rather diffuse across the membrane through an essentially hydrophilic pathway; although, the solvation fluctuation plays a significant role in the water filled pore formation across the membrane under the transmembrane voltage.

The mechanism of the voltage-sensor domain translocation across the lipid membrane is inhomogeneous and complex, and our proposed water-pore pathway mechanism does not necessary exclude the conventional mechanisms [7,13,19,20,105,106]. Although we have observed a 40±10% probability of THC state occurrence in the recorded active ion channel activation events, there are portions of THC state occurrences that do not follow with a measurable active ion channel formation. Furthermore, certain portion of ion channel formation events oc-

curs without any observable THC state. Possible reasons might be: (1) the voltage sensor domain diffuses across the lipid membrane solely as transmembrane voltage driven, consistent with the conventional mechanism; (2) the hydrophilic water-pore pathway existence is too transient to be detected by either the fluorescence imaging or the electrophysiological conductance recording; (3) the water-pore pathway associated with the voltage sensor domain diffusion is transient and fluctuating together with peptide solvation fluctuations, and in the course of the polypeptide domain relocation across the membrane, the hydrophilic water-pore pathway never fully formed at any time but formed averagely in time. Definitely, additional investigations are needed to resolve the ion channel formation and activation events without a measureable THC state occurrence, and the complexity and inhomogeneity of the molecular dynamics must be considered in the overall process of voltage sensor domain translocation across the lipid membrane under a constant transmembrane voltage. Furthermore, the membrane local environment is definitely even more complex and inhomogeneous, which most likely involves more complex mechanism with multiple pathways. However, such further studies are beyond the scope of this reported work. Nevertheless, the water-pore pathway formation mechanism proposed in this work is significant and important in case of colicin ion channel formation, and the mechanism provides a profound physical nature of a voltage sensor polypeptide domain motions and voltage-gated ion channel activities under a transmembrane voltage.

4. CONCLUSIONS

We have applied a combined fluorescence imaging and electric conductance recording approach, correlating with computational molecular dynamics simulations to study the mechanism and dynamics of colicin Ia charged domain translocation across the lipid bilayer in the activation of the colicin ion channel. Our results reveal a new mechanism that the activation of the ion channel is due to voltage sensor domain diffusion across lipid bilayer membrane under transmembrane voltage. We have identified a significant probability of the colicin ion channel activation

events are associated with a high conductance state resulting from the formation of a water-pore in the lipid bilayer as large as ~15 Å diameter. This experimental result is supported and further identified from our molecular dynamics simulations. The water-pore pathway provides an energetically favorable polar pathway for the charged voltage-sensor α-helices to cross the lipid bilayer in order to form the activated channel configuration. The most significant result of our MD simulation is that the location of the water-pore formation in the membrane is always non-random and right under the voltage sensor peptide domain. Ultimately, charged peptide solvation energetics and dynamics play a critical role in the water filled pathway formation. Here we are able to shed a light on the fundamental translocation mechanism of a voltage sensor charged polypeptide domain under an external electric field: the charged polypeptide domain facilitates the formation of a water-pore pathway in the membrane and diffuses through that hydrophilic pathway across the membrane, thereby forming the activated ion channel. Although the results presented here are based on the study of colicin Ia as a model system, the knowledge obtained here can have significant implications on understanding other voltage gated ion channel activation mechanism and dynamics in living cells.

14

[1] B. Hille, *Ionic channels of excitable membranes,* Sinauer Associates Sunderland, MA (1984).

[2] W. A. Catterall, Science **242**, 50 (1988).

[3] H. R. Leuchtag, *Voltage-sensitive ion channels: biophysics of molecular excitability*, Springer (2008).

[4] S. L. Slatin, X. Qiu, K. S. Jakes, and A. Finkelstein, Nature **371**, 158 (1994).

[5] X. Q. Qiu, K. S. Jakes, A. Finkelstein, and S. L. Slatin, J. Biol. Chem. **269**, 7483 (1994).

[6] X. Q. Qiu, K. S. Jakes, P. K. Kienker, A. Finkelstein, and S. L. Slatin, J. Gen. Physiol. **107**, 313 (1996).

[7] Y. Jiang, V. Ruta, J. Chen, A. Lee, and R. MacKinnon, Nature **423**, 42 (2003).

[8] B. Chanda, and F. Bezanilla, J. Gen. Physiol. **120**, 629 (2002).

[9] W. Treptow, B. Maigret, C. Chipot, and M. Tarek, Biophys. J. **87**, 2365 (2004).

[10] H. Vogel, L. Nilsson, R. Rigler, S. Meder, G. Boheim, W. Beck, H.-H. Kurth, and G. Jung, Eur. J. Biochem. **212**, 305 (1993).

[11] S. Dorairaj, and T. W. Allen, Proc. Natl. Acad. Sci. **104**, 4943 (2007).

[12] M. Grabe, H. Lecar, Y. N. Jan, and L. Y. Jan, Proc. Natl. Acad. Sci. **101**, 17640 (2004).

[13] T. Hessa, H. Kim, K. Bihlmaier, C. Lundin, J. Boekel, H. Andersson, I. Nilsson, S. H. White, and G. von Heijne, Nature **433**, 377 (2005).

[14] L. Hong, M. M. Pathak, I. H. Kim, D. Ta, and F. Tombola, Neuron **77**, 274 (2013).

[15] K. Matsuzaki, O. Murase, N. Fujii, and K. Miyajima, Biochemistry **34**, 6521 (1995).

[16] K. Bhattacharyya, ChemComm 2848 (2008).

[17] D. K. Das, T. Mondal, U. Mandal, and K. Bhattacharyya, ChemPhysChem **12**, 814 (2011).

[18] U. Anand, C. Jash, and S. Mukherjee, Phys. Chem. Chem. Phys. **13**, 20418 (2011).

[19] G. Yellen, Nature **419**, 35 (2002).

[20] G. Yellen, Quart. Rev. Biophys. **31**, 239 (1998).

[21] C. M. Armstrong, and B. Hille, Neuron **20**, 371 (1998).

[22] J. Konisky, Ann. Rev. Microbiol. **36**, 125 (1982).

[23] P. K. Kienker, K. S. Jakes, and A. Finkelstein, J. Gen. Physiol. **116**, 587 (2000).

[24] K. S. Jakes, P. K. Kienker, and A. Finkelstein, Quart. Rev. Biophys. **32**, 189 (1999).

[25] P. Elkins, A. Bunker, W. A. Cramer, and C. V. Stauffacher, Structure **5**, 443 (1997).

[26] M. Wiener, D. Freymann, P. Ghosh, and R. M. Stroud, Nature **385**, 461 (1997).

[27] S. L. Slatin, and P. K. Kienker, Colicin channels and protein translocation. Parallels with diphtheria toxin. In *Pore forming peptides and protein toxins* (Menestrina, G., Ed.), pp 102, Taylor and Francis: London (2003).

[28] W. A. Cramer, J. B. Heymann, S. L. Schendel, B. N. Deriy, F. S. Cohen, P. A. Elkins, and C. V. Stauffacher, Ann. Rev. Biophys. Biomol. Struct. **24**, 611 (1995).

[29] R. A. Nogueira, and W. A. Varanda, J. Membrane Biol. **105**, 143 (1988).

[30] P. Ghosh, S. F. Mel, and R. M. Stroud, J. Membrane Biol. **134**, 85 (1993).

[31] R. Stroud, Curr. Opin. Struct. Biol. **5**, 514 (1995).

[32] W. Luo, X. Yao, and M. Hong, J. Am. Chem. Soc. **127**, 6402 (2005).

[33] P. K. Kienker, X. Qiu, S. L. Slatin, A. Finkelstein, and K. S. Jakes, J. Membrane Biol. 157, 27 (1997).

[34] N. Yang, A. L. George, and R. Horn, Neuron **16**, 113 (1996).

[35] F. Tombola, M. Pathak, and E. Y. Isacoff, Annu. Rev. Cell Dev. Biol. **22**, 23 (2006).

[36] S. P. Rajapaksha, X. Wang, and H. P. Lu, Anal. Chem. **85**, 8951 (2013).

[37] G. S. Harms, G. Orr, M. Montal, B. D. Thrall, S. D. Colson, and H. P. Lu, Biophys. J. 85, 1826 (2003).

[38] H. P. Lu, L. Y. Xun, and X. S. Xie, Science **282**, 1877 (1998).

[39] G. Harms, G. Orr, and H. P. Lu, Appl. Phys. Lett. **84**, 1792 (2004).

[40] B. Hess, C. Kutzner, D. van der Spoel, and E. Lindahl, J. Chem. Theory Comput. 4, 435 (2008).

[41] D. van der Spoel, E. Lindahl, B. Hess, G. Groenhof, A. E. Mark, and H. J. C. Berendsen, J. Comp. Chem. **26**, 1701 (2005).

[42] E. Lindahl, B. Hess, and D. van der Spoel, J. Mol. Model **7**, 306 (2001).

[43] H. J. C. Berendsen, D. van der Spoel, and R. Van Drunen, Comp. Phys. Comm. **91**, 43 (1995).

[44] J. Hermans, H. J. C. Berendsen, W. F. Van Gunsteren, and J. P. M. Postma, Biopolymers **23**, 1513 (1984).

[45] O. Berger, O. Edholm, and F. Jahnig, Biophys. J. **72**, 2002 (1997).

[46] D. P. Tieleman, and H. J. C. Berendsen, J. Chem. Phys. **105**, 4871 (1996).

[47] http://lipidbook.bioch.ox.ac.uk/package/show/id/20.html

[48] C. Kandt, W. L. Ash, and D. P. Tieleman, Methods **41**, 475 (2007).

[49] H. J. C. Berendsen, J. P. M. Postma, W. F. van Gunsteren, and J. Hermans, Intermolecular Forces 11, 331 (1981).

[50] S. A. Nosé, J. Chem. Phys. **81**, 511 (1984).

[51] W. G. Hoover, Phys. Rev. A **31**, 1695 (1985).

[52] M. Parrinello, and A. Rahman, J. Appl. Phys. **52**, 7182 (1981).

[53] S. Nosé, and M. L. Klein, Mol. Phys. **50**, 1055 (1983).

[54] B. Hess, H. Bekker, H. J. C. Berendsen, J. G. E. M. Fraaije, J. Comp. Chem. **18**, 1463 (1997).

[55] T. Darden, D. York, and L. Pedersen, J. Chem. Phys. **98**, 10089 (1993).

[56] W. Humphrey, A. Dalke, and K. Schulten, J. Mol. Graphics **14**, 33 (1996).

[57] F. Ryttsén, C. Farre, C. Brennan, S.G. Weber, K. Jardemark, D.T. Chiu, and O. Orwar, Biophys. J. **79**, 1993 (2000).

[58] H. P. Lu, Acc. Chem. Res. **38**, 557 (2005).

[59] H. P. Lu, Methods Cell Biol. **90**, 435 (2008).

[60] T. Ide, M. Hirano, Y. Takeuchi, Ion Channels. Single Molecule Dynamics in Life Science 87 (2009).

[61] M. Andersson, J. A. Freites, D. J. Tobias, S. H. White, J. Phys. Chem. B **115**, 8732 (2011).

[62] D. Krepkiy, M. Mihailescu, J. A. Freites, E. V. Schow, D. L. Worcester, K. Gawrisch, D. J. Tobias, S. H. White, and K. J. Swartz, Nature **462**, 473 (2009).

[63] V. Yarov-Yarovoy, P. G. DeCaen, R. E. Westenbroek, C.-Y. Pan, T. Scheuer, D. Baker, and W. A. Catterall, Proc. Natl. Acad. Sci. **109**, E93 (2012).

[64] E. C. McCusker, C. Bagnéris, C. E. Naylor, A. R. Cole, N. D'Avanzo, C. G. Nichols, and Wallace, B. A. Nat. Commun. **3**, 1102 (2012).

[65] J. C. Gumbart, I. Teo, B. Roux, and K. Schulten, J. Am. Chem. Soc. **135**, 2291 (2013).

[66] F. Khalili-Araghi, E. Tajkhorshid, B. Roux, and K. Schulten, Biophys. J. **102**, 258 (2012).

[67] M. O. Jensen, V. Jogini, D. W. Borhani, A. E. Leffler, R. O. Dror, and D. E. Shaw, Science **336**, 229 (2012).

[68] Z. Lai, K. Zhang, and J. Wang, Phys. Chem. Chem. Phys. **16**, 6486 (2014).

[69] X. Zheng, and J. Wang, PLoS Comput Biol 11(4): e1004212 (2015).

[70] T. B. Woolf, and B. Roux, Proc. Nalt. Acad. Sci. USA **91**, 11631 (1994).

[71] L. Saiz, and M. L. Klein, Acc. Chem. Res. **35**, 482 (2002).

[72] M. B. Ulmschneider, J. P. Ulmschneider, N. Schiller, B. A. Wallace, G. von Heijne, and S. H. White, Nat. Commun. **5**, 4863 (2014).

[73] W. L. Ash, M. R. Zlomislic, E. O. Oloo, and D. P. Tieleman, Biochimica et Biophysica Acta-Biomembranes **1666**, 158 (2004).

[74] L. R. Forrest, and M. S. Sansom, Curr. Opin. Struct. Biol. **10**, 174 (2000).

[75] S. K. Kandasamy, and R. G. Larson, Biophys. J. **90**, 2326 (2006).

[76] S. S. Deol, P. J. Bond, C. Domene, and M. S. P. Sansom, Biophys. J. **87**, 3737 (2004).

[77] L. Prieto, and T. Lazaridis, Proteins **79**, 126 (2011).

[78] D. Chandler, Introduction to Modern Statistical Mechanics. Oxford University Press: New York, U.S.A (1987).

[79] A. A. Aleksandrov, and J. R. Riordan, FEBS Lett. 431, **97** (1998).

[80] See Supplemental Material at [*URL will be inserted by publisher*] for the analysis of conductance trajectories at 50 mV and 100 mV transmembrane voltage, simulation snap shots of solvated DPhPC bilayer under transmembrane electric field, colicin Ia in DPhPC bilayer after the transmembrane electric field is switched off, colicin Ia in DPhPC bilayer without any transmembrane electric field and the movies generated from the simulations snap shots of colicin Ia in DPhPC bilayer under the transmembrane electric field.

[81] M. L. Scalley, and D. Baker, Proc. Nalt. Acad. Sci. USA **94**, 10636 (1997).

[82] T.-L. Kuo, S. Garcia-Manyes, J. Li, I. Barel, H. Lu, B. J. Berne, M. Urbakh, J. Klafter, and J. M. Fernandez, Proc. Nalt. Acad. Sci. USA **107**, 11336 (2010).

[83] H. Frauenfelder, S. G. Sligar, and P. G. Wolynes, Science **254**, 1598 (1991).

[84] H. Frauenfelder, and P. G. Wolynes, Physics Today **47**, 58 (1994).

[85] O. V. Krasilnikov, J. B. Da Cruz, L. N. Yuldasheva, W. A. Varanda, and R. A. Nogueira, J. Membrane Biol. **161**, 83 (1998).

[86] L. M. Harriss, B. Cronin, J. R. Thompson, and M. I. Wallace, J. Am. Chem. Soc. **133**, 14507 (2011).

[87] W. F. D. Bennett, and D. P. Tieleman, Acc. Chem. Res. **47**, 2244 (2014).

[88] J. Lin, and A. Alexander-Katz, ACS Nano **7**, 10799 (2013).

[89] B. Song, H. Yuan, S. V. Pham, J. J. Cynthia, and S. Murad, Langmuir **28**, 16989 (2012).

[90] J. Gumbert, C. Chipot, and K. Schulten, Proc. Nalt. Acad. Sci. USA **108**, 3596 (2011).

[91] A. C. V. Johansson, and E. Lindahl, Proc. Nalt. Acad. Sci. USA **106**, 15684 (2009).

[92] N. A. Berglund, T. J. Piggot, D. Jefferies, R. B. Sessions, P. J. Bond, and S. Khalid, PLoS Comput Biol 11(4): e1004180 (2015).

[93] A. C. V. Johansson, and E. Lindahl, Biophys J. **91**, 4450 (2006).

[94] E. Strandberg, and J. A. Killian, FEBS Letters **544**, 69 (2003).

[95] W. J. Allen, J. A. Lemkul, and D. R. Bevan, J. Comp. Chem. **30**, 1952 (2008).

[96] J. A. Freites, D. J. Tobias, G. von Heijne, and S. H. White, Proc. Natl. Acad. Sci. **102**, 15059 (2005).

[97] D. P. Tieleman, H. Leontiadou, A. E. Mark, and S. J. Marrink, J. Am. Chem. Soc. **125**, 6382 (2003).

[98] D. P. Tieleman, BMC Biochemistry **5**:10 (2004).

[99] L. Wang, R. A. Friesner, and B. J. Berne, Faraday Discuss. **146**, 247 (2010).

[100] J. E. Ladbury, Chem. Biol. **3**, 973 (1996).

[101] S. K. Buchanan, P. Lukacik, S. Grizot, R. Ghirlando, M. M. Ali, T. J. Barnard, K. S. Jakes, P. K. Kienker, and L. Esser, EMBO J **26**, 2594 (2007).

[102] J. Kyte, and R. F. Doolittle, J. Mol. Biol. **157**, 105 (1982).

[103] M. Tarek, Biophys. J. **88**, 4045 (2005).

[104] L. Chen, X. Li, L. Gao, and W. Fang, J. Phys. Chem. B **119**, 850 (2015).

[105] Y. Jiang, A. Lee, J. Chen, V. Ruta, M. Cadene, B. T. Chait, and R. MacKinnon, Nature **423**, 33 (2003).

[106] T. Hessa, S. H. White, G. von Heijne, Science **307**, 1427 (2005).